H_2O_2-Aided One-Pot Hydrothermal Synthesis of Nanocrystalline $LiMn_2O_4$ Cathode for Lithium Batteries

K. Sathiyaraj, Gangulibabu, D. Bhuvaneswari, N. Kalaiselvi, and A. John Peter

***Abstract*—A simple and H_2O_2-aided hydrothermal (HDT) method has been deployed to synthesize nanocrystalline $LiMn_2O_4$ at 140 °C using an in-house-made hydrothermal reaction vessel. Phase pure, highly crystalline, and uniformly distributed nanorods of 100 nm length are obtained from the H_2O_2 aided exothermic oxidation of precursor mix, especially when an excess amount of lithium (Li: Mn as 2:1) is used. The crystalline nature of $LiMn_2O_4$ and the growth of nanorods along (111) crystallographic direction are understood from powder x-ray diffraction (PXRD) and selective area electron diffraction (SAED) analysis, respectively. The synthesized cathode exhibited an initial capacity of 118 mAh g^{-1} with a slightly higher initial capacity fade (9%) and a progressively stabilized (<3% capacity fade) specific capacity behavior upon cycling. An equivalent circuit model is proposed to fit with the observed impedance behavior of $LiMn_2O_4$ cathode. The exploitation of low temperature assisted one-pot hydrothermal synthesis to prepare nanocrystalline $LiMn_2O_4$ compound and the suitability of the same to exhibit better lithium intercalation behavior are demonstrated in this communication.**

***Index Terms*—Hydrothermal method, $LiMn_2O_4$, lithium batteries, nanocrystalline cathode.**

I. Introduction

SPINEL $LiMn_2O_4$, possessing a 3-D interstitial space for Li^+ ion transport and bestowed with advantages like ecobenign nature, economic viability, and the abundant availability of manganese resource is one of the potential cathodes exploited in rechargeable lithium battery applications. However, the major limitation of $LiMn_2O_4$ electrode material, viz., unacceptable capacity fade upon electrochemical cycling is due to factors such as: 1) fracture of the particle surface due to local Jahn-Teller distortions at high rates of discharge [1]; 2) dissolution of manganese from lithiated [2] and delithiated spinels [3]; 3) electrolyte oxidation on the spinel surface [4]; 4) cation mixing, or Li/Mn site exchange [5]; 5) loss of oxygen from the spinel [6]; and 6) structural failure in the two-phase reaction region [7]. Several attempts are being made to alleviate the aforesaid problems, which include the selection of compatible electrolytes, coating of spinel particles with chemically stable species, tuning of physical parameters such as phase purity, particle size, surface area, etc., by way of adopting optimized synthesis procedure and partial substitution of suitable dopants for manganese/oxygen ions [8]. Among these approaches, the effect of synthesis methodology has a direct impact on morphology, size, and distribution of particles that are the critical parameters to facilitate faster lithium ion diffusion kinetics [9].

Spinel lithium manganese oxide, when prepared by solid-state reaction, produces inhomogeneity of composition, irregular grain shape, and larger grain size. Solution-assisted synthesis methods such as sol-gel [10], combustion [11], pechini [12], and emulsion-drying [13] approaches are reported to form submicron sized $LiMn_2O_4$ particles, due to the atomic level distribution of reactants in the homogenous solution. On the other hand, nanocrystalline $LiMn_2O_4$ material with larger surface-to-volume ratio that allows for larger electrode-electrolyte contact and by reducing the lithium ion diffusion path length is reported to exhibit an improved electrochemical performance [14] than conventional $LiMn_2O_4$ cathodes [15]. Toward this direction, template method [16], hydrothermal solid-state method [17], self-seeded surfactant directed growth process [18] are reported to form growth controlled $LiMn_2O_4$ nanoparticles [19].

Generally, phase pure and homogenous distribution of nanocrystalline particles with larger surface area is desired for any lithium intercalating cathode material to exhibit better electrode performance [9]. Even though solution-assisted synthesis approaches of the aforesaid category are known for phase pure, homogenous distribution of particles and formation of submicron particles, requirement of higher calcination temperature in all these methods [10]–[12] is unavoidable. On the other hand, a low temperature requiring hydrothermal method is chosen for the present study, which is an energy saving approach to prepare nanocrystalline powders and thus gains importance. In other words, a low temperature involving H_2O_2-based hydrothermal approach has been followed to synthesize nanocrystalline $LiMn_2O_4$ cathode, wherein a perfect control over particle size and surface morphology is obtained by way of adjusting the total internal pressure of the in-house made hydrothermal reaction vessel (Fig. 1). Not requiring an autoclave for pressure

Manuscript received December 9, 2010; revised August 2, 2011; accepted September 26, 2011. Date of publication November 15, 2011; date of current version March 9, 2012. This work was supported by CSIR under grant for IAP-04 project through 11th five-year program. The review of this paper was arranged by Associate Editor M. M. De Souza.

K. Sathiyaraj is with the Nanotechnolgy division, Periyar Maniammai University, Thanjavur – 613 403, India. K. Sathiyaraj did this work while he was with ECPS, Central Electrochemical Research Institute, Karaikudi – 630 006, India (e-mail: k.sathiyaraj14@gmail.com).

G. D. Bhuvaneswari and N. Kalaiselvi are with the ECPS, Central Electrochemical Research Institute, Karaikudi – 630 006, India (e-mail: gangulababuredy@gmail.com; bhuvanarajj@gmail.com; kalakanth2@yahoo.com).

A. J. Peter is with the Department of Physics, Government Arts and Science College, Melur-625 106, India (e-mail: a.john.peter@gmail.com).

Color versions of one or more of the figures in this paper are available online at http://ieeexplore.ieee.org.

Digital Object Identifier 10.1109/TNANO.2011.2171359

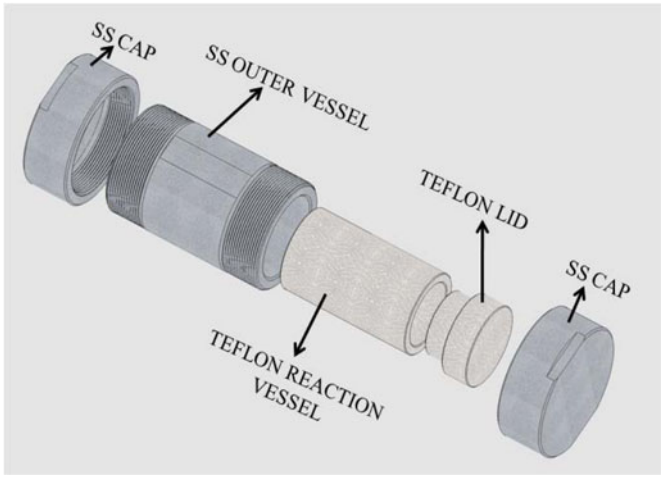

Fig. 1. In-house made hydrothermal reaction vessel.

adjustments in the hydrothermal synthesis, the currently used in-house made reaction vessel is helpful in maintaining the required internal pressure by way of keeping an optimum volume of hot solution containing H_2O_2 and precursor mix. Further, unlike the solvo thermal preparation of $LiMn_2O_4$ at 750 °C that involves a two stage synthesis mechanism or carbonate precursor based solid state synthesis approach that requires a temperature of 700 °C to form $LiMn_2O_4$ compound [20], the present study deals with a simplified hydrothermal approach, wherein nanocrystalline $LiMn_2O_4$ with a homogenous distribution of nanorods of 100 nm length has been obtained more readily at a temperature as low as 140 °C. In short, the study has a major focus on the cost-effective hydrothermal synthesis approach to prepare nanocrystalline $LiMn_2O_4$ compound and an investigation on the suitability of thus prepared $LiMn_2O_4$ cathode for application in rechargeable lithium batteries.

II. Experimental Details

A. Synthesis

Spinel $LiMn_2O_4$ was synthesized by a low temperature hydrothermal method with starting materials such as LiOH (Merck), $Mn(NO_3)_2$ (Merck), and H_2O_2 (Alfa Aesar). An aqueous solution of 1M LiOH and 3.5% of H_2O_2 was added drop wise in to a solution of 0.5M $Mn(NO_3)_2$ under vigorous stirring. A black viscous solution was obtained, which was then transferred to an in-house made hydrothermal setup (Fig. 1) and kept aside at room temperature for 2 h. The total volume of precursor solution was optimized and maintained as 80% of the total capacity of the hydrothermal vessel in order to realize an internal pressure of the order of ~25 MPa, needed for the reaction. Subsequently, the setup was sealed tightly and transferred to a preheated oven and heat treated at 140 °C for 12 h. The oven was then allowed to cool to room temperature and the formed precipitate was separated and washed twice with double distilled water. The washed precipitate was dried at 110 °C for 10 h and ground well. The resultant nanocrystalline $LiMn_2O_4$ compound was subjected to systematic physical and electrochemical characterizations. Possible mechanism involved in the formation of $LiMn_2O_4$ is given as under:

$$Mn(NO_3)_2 + H_2O_2 \rightarrow Mn(OH)_2 + 2NO_2 + O_2 \uparrow$$

$$Mn(OH)_2 + 1/2\,H_2O_2 \rightarrow MnOOH + H_2O$$

$$2MnOOH + LiOH + 1/2H_2O_2 \rightarrow LiMn_2O_4 + 2H_2O.$$

B. Physical and Electrochemical Characterizations

Phase characterization was done by powder X-ray diffraction technique on a Philips 1830 X-ray diffractometer using Ni-filtered Cu K_α radiation ($\lambda = 1.54$ A°) in the 10–90° range at a scan rate of 0.04°/s. The surface morphology and microstructure of synthesized samples were examined by scanning electron microscopy (SEM, HITACHI S–3000 H, and Japan) and transmission electron microscopy (TEM, FEI-Tecnai-20G2). The chemical composition of $LiMn_2O_4$ compound was confirmed by X-ray photoelectron spectroscopy (XPS, VG electron spectroscopy) using an Mg Kα excitation source. Fourier transform infrared spectroscopy (FTIR) was performed on a Perkin–Elmer Paragon-500 FTIR spectrophotometer using a pellet containing a mixture of KBr and the response of active material in the region 400–1200 cm^{-1} was recorded. Room temperature electrochemical studies such as cyclic voltametry (CV) and electrochemical impedance spectroscopy (EIS) measurements were performed using an auto lab electrochemical workstation, wherein CV scan rate was fixed as 0.5 mV/s and the impedance analysis was done over a frequency range of 100 KHz–0.1 Hz. Electrochemical charge–discharge study was carried out using Arbin instruments (BT 2000).

C. Electrode Preparation and Coin Cell Fabrication

Coin cell was fabricated using HDT synthesized $LiMn_2O_4$ material as cathode, lithium metal as anode, and a solution consisting of 1M $LiPF_6$ dissolved in 1:1 v/v EC: DEC as electrolyte along with celgard separator. The detailed procedure for electrode preparation and coin cell fabrication is described elsewhere [21].

III. Result and Discussion

A. Phase Analysis—PXRD Studies

Fig. 2 shows the XRD pattern recorded for $LiMn_2O_4$ compound synthesized via HDT approach with a slight variation in the reaction conditions, viz., usage of stoichiometric and excess amount of lithium in the precursor mix. The PXRD patterns of $LiMn_2O_4$ compound synthesized with the stoichiometric amount of lithium [Fig. 2(a) and (b)] correspond to the formation of MnO_2 compound (JCPDS No: 65-2821), wherein the appearance of (111) peak at $2\theta = 18.9°$, corresponding to the presence of cubic spinel $LiMn_2O_4$ is missing. Hence, the partial occupation of lithium ions in the Li site of $LiMn_2O_4$ [22], resulting from the washing and nonwashing of precipitates obtained from the usage of stoichiometric amount of lithium in HDT method is understood. Further, it is obvious from the PXRD pattern of Fig. 2(a) and (b) that an excess concentration of lithium in

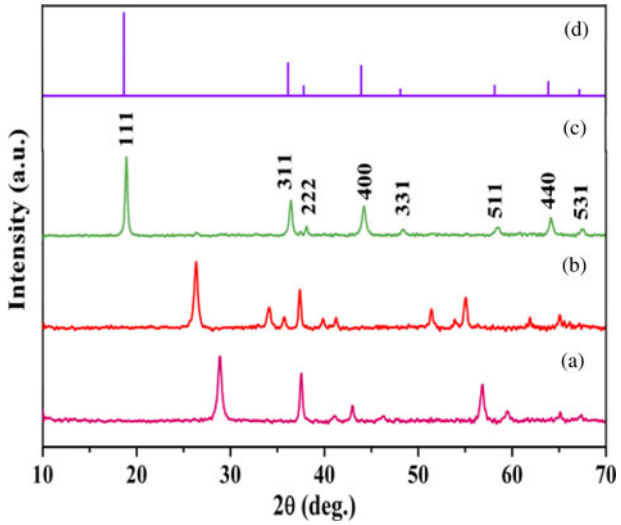

Fig. 2. XRD pattern of $LiMn_2O_4$ synthesized using hydrothermal method with different conditions: (a) Stoichiometric amount of lithium with the washing of precipitate. (b) Stoichiometric amount of lithium without washing the precipitate. (c) Excess concentration of lithium with washing of formed precipitate. (d) JCPDS file no. 88–1030.

TABLE I
PHYSICAL PARAMETERS OF $LiMn_2O_4$ CALCULATED FROM XRD

Lattice Constant (a) (A°)		Cell Volume $(A°)^3$		Avg. Crystal Size (nm)	Stokes Strain
Experimental	JCPDS	Experimental	JCPDS	20.89	6.734 x 10^{-3}
8.19	8.24	549.94	559.13		

the precursor mix is essential to obtain phase pure $LiMn_2O_4$ compound, especially when HDT method is deployed. Accordingly, the PXRD pattern of spinel $LiMn_2O_4$ synthesized from a mixture containing 2:1 molar ratio of Li:Mn precursor matches exactly [Fig. 2(c)] with the standard JCPDS pattern (File No: 88-1030), confirming the phase pure formation of title compound.

All the Bragg peaks were indexed to the cubic spinel structure of $LiMn_2O_4$ with an Fd3m space group [23]. The peak broadening observed in all the three attempts of HDT method [Fig. 2(a)–(c)] is attributed to the formation of nanocrystalline $LiMn_2O_4$ compound. Particularly, Fig. 2(c) corresponds to the formation of nanocrystalline $LiMn_2O_4$ compound with an average grain size of 30 nm, as derived from the Scherrer equation. The calculated values of lattice parameter and physical constants are in good agreement with the reported values (Table I).

Interestingly, the (111) peak has smaller FWHM (full width at half maximum) value and larger crystallite size compared to other peaks, which is an indication that the formed nanoparticles grow preferentially along the (111) direction to form nanorods [17]. Further, presence of intense and sharp peaks [Fig. 2(c)] evidences the crystalline nature [24] of $LiMn_2O_4$ compound prepared at a temperature as low as 140 °C. The internal pressure created within the in-house made hydrothermal vessel due to the H_2O_2 −aided exothermic oxidation of precursor mix is believed

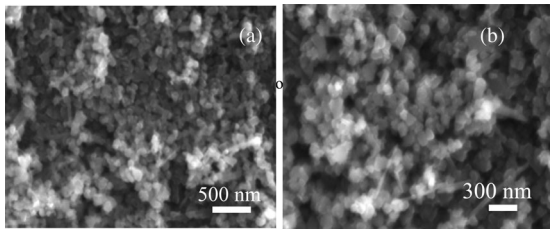

Fig. 3. Fig. 3 SEM images of $LiMn_2O4$ synthesized by HDT method showing a) uniform distribution of particles. b) growth controlled particles.

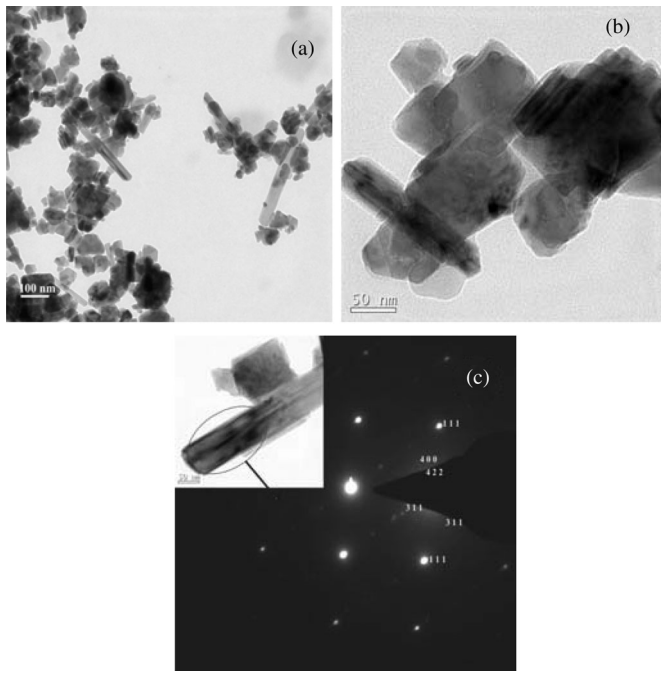

Fig. 4. TEM image and SAED pattern recorded for $LiMn_2O_4$ nanorod.

to impart crystallinity to the final product [25] at 140 °C itself, which is noteworthy.

B. Surface Morphology and Particle Size—SEM and TEM Studies

Fig. 3(a) evidences the formation and uniform distribution of size-reduced cubic particles possessing definite inter-particle grain boundaries. Presence of growth-controlled nanorods [Fig. 3(b)] is also seen from the SEM image, which is noteworthy.

TEM images [Fig. 4(a) and (b)] of $LiMn_2O_4$ compound confirm the presence of nanorods possessing ∼100 nm length and a diameter 50 nm. The controlled growth of nanorods along the (111) crystallographic direction is confirmed from SAED results [26], which is in agreement with the XRD results. Further, the crystal lattice parameter values calculated for (111), (400), (422), and (311) planes in SAED are found to match well with those calculated from XRD results (Table II).

TABLE II
COMPARISON OF PHYSICAL PARAMETERS DERIVED FROM XRD AND SAED (TEM) ANALYSIS

Plane	d – Spacing (A^0)		
	SAED(TEM)	XRD	JCPDS
1 1 1	4.58	4.63	4.76
3 1 1	2.52	2.46	2.48
4 0 0	2.1	2.05	2.06
4 2 2	1.64	1.66	1.68
Lattice constant a (A°)	8.07	8.19	8.24
Cell volume $(A°)^3$	525.89	549.94	559.13

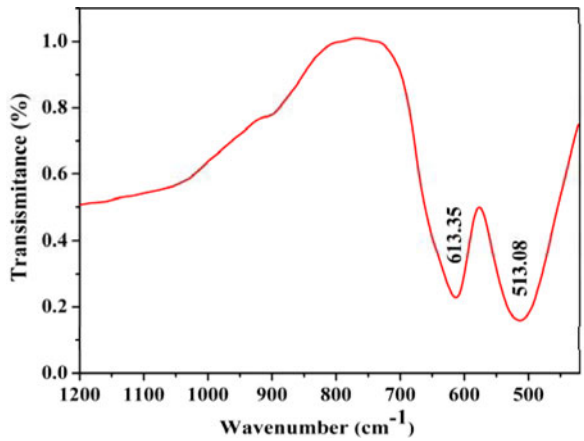

Fig. 5. FTIR spectrum of $LiMn_2O_4$ compound.

C. Cationic Environment—FTIR Analysis

FTIR spectroscopy is an effective technique in differentiating the ordered versus disordered structures of the $LiMn_2O_4$ cathode materials. Fig. 5 shows the room temperature FTIR absorption spectra of spinel $LiMn_2O_4$ that consists of a series of broad bands between 450 and 650 cm^{-1}, corresponding to the F_{1u} symmetry modes [27]. However, the FTIR spectrum of $LiMn_2O_4$ spinel is dominated by two strong absorption bands at 613 and 513 cm^{-1}, corresponding to the displacement of oxide ions and are attributed primarily to the asymmetric stretching modes of MnO_6 octahedra. It is obvious that such vibrations are not resulting from an isolated MnO_6 octahedra, because the MnO_6 octahedra of spinel $LiMn_2O_4$ are connected to other MnO_6 octahedra and LiO_4 tetrahedra [28]. Since the Li-O related vibrations lie far below 400 cm^{-1} [10], the same is not discussed in this communication.

D. Oxidation State of Elements—XPS Study

The chemical composition of spinel $LiMn_2O_4$ has been examined by XPS, as the measurement is suitable for quantitative analysis of Li–Mn–O compounds, wherein a first-order process

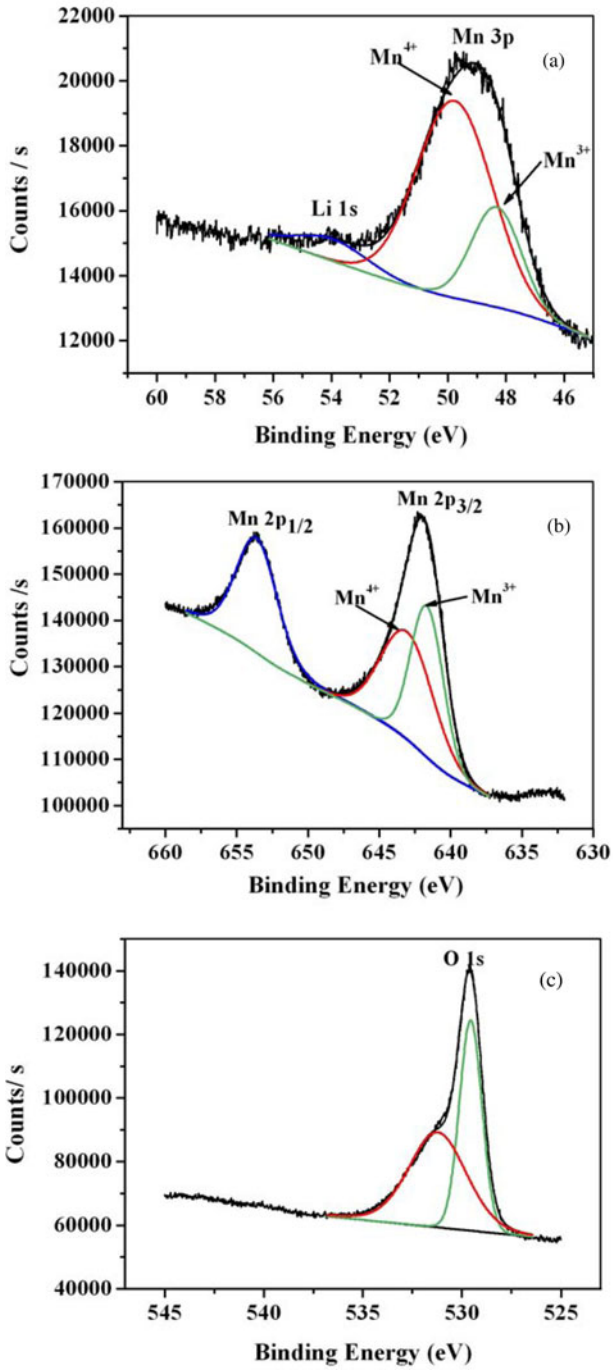

Fig. 6. XPS spectra of (a) Li 1 s and Mn 3p, (b) Mn 2p and (c) O 1 s of $LiMn_2O_4$ compound.

is involved in the photoelectron emission. Quantitative analysis of $LiMn_2O_4$ is made from the integrated intensities of the Mn 2p and Li 1 s lines, which are observed with the peaks attributed to oxygen in the XPS spectrum. Fig. 6 displays the deconvoluted XPS spectra of Mn 2p, O 1 s, Li 1 s, and Mn 3p core-level photoemission peaks for spinel $LiMn_2O_4$. The Li 1 s core level of $LiMn_2O_4$ has a low intensity with a binding energy located at 54.0 eV [Fig. 6(a)], which is close to that of Li metal (54.6 eV) [29]. The deconvolution carried out in the peak of

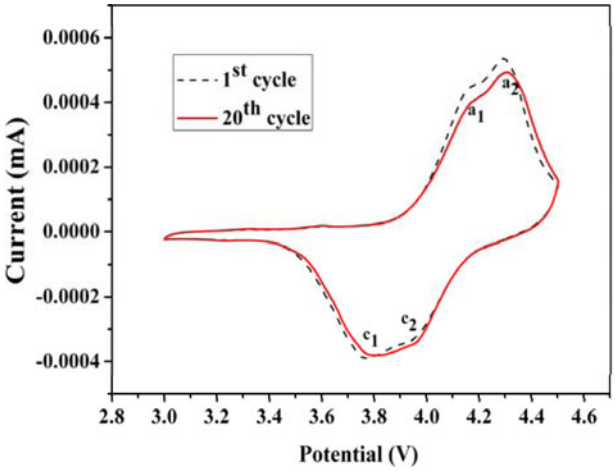

Fig. 7. Cyclic voltammogram of $LiMn_2O_4$ cathode upon cycling.

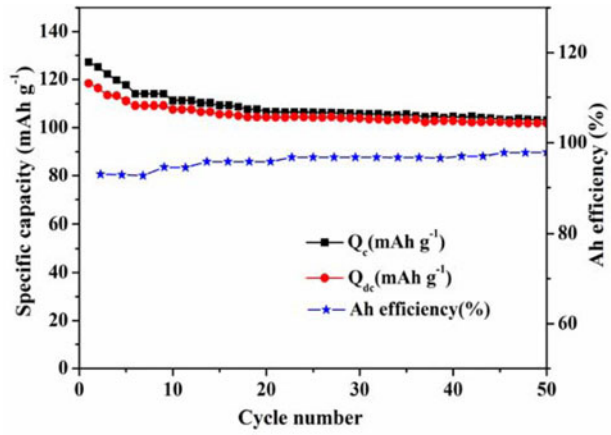

Fig. 8. Cycling performance of spinel $LiMn_2O_4$ cathode.

Mn 3p core level shows peaks of Mn^{3+} and Mn^{4+} at 48.3 and 49.8 eV [Fig. 6(a)], respectively. Similarly, the deconvoluted Mn $2p_{3/2}$ peak in $LiMn_2O_4$ [Fig. 6(b)] also exhibits two peaks at 641.6 and 643.0 eV, corresponding to the presence of Mn^{3+} and Mn^{4+}, respectively [30].

The observed energy separation of 11.5 eV between the Mn $2p_{3/2}$ and Mn $2p_{1/2}$ states and the intensity ratio 2:1 of Mn $2p_{3/2}$ and Mn $2p_{1/2}$ confirm that the $LiMn_2O_4$ compound synthesized using HDT method is in agreement with the stoichiometric spinel material [31]. Fig. 6(c) shows that peaks at 529.6 and 531.1 eV are related to the line of O 1 s core level, which is also in agreement with the stoichiometric formation of $LiMn_2O_4$.

E. Cyclic Voltammetry Studies

Fig. 7 shows the cyclic voltammogram (CV) of $LiMn_2O_4$ cathode recorded at a sweep rate of 0.1 mV s^{-1} for about 20 cycles.

The CV of $LiMn_2O_4$ cathode consists of two anodic (a_1 and a_2) and two cathodic (c_1 and c_2) peaks [32], [33], corresponding to the two-step reversible deintercalation and intercalation of lithium according to the following reactions:

$$LiMn_2O_4 \leftrightarrow Li_{0.5}Mn_2O_4 + 0.5Li^+ + 0.5e^- \quad (1)$$

and

$$Li_{0.5}Mn_2O_4 \leftrightarrow \lambda{-}MnO_2 + 0.5Li^+ + 0.5e^-. \quad (2)$$

The first pair of peaks, viz., a_1 and c_1 at 4.2 and 3.8 V corresponding to (1) is attributed to the removal/addition of Li ions from/into a half of the tetrahedral sites in which Li/Li^+ interaction occurs [33], [34]. The second redox pair, viz., a_2 and c_2 observed at 4.3 and 3.9 V corresponding to (2) is attributed to the intercalation/deintercalation of lithium in to the other half of the tetrahedral sites [35]–[37]. It is well known that these processes are accompanied by the reversible Mn^{3+}/Mn^{4+} redox reactions [32] and, hence, the cycling reversibility of $LiMn_2O_4$ cathode could be understood. The potential difference corresponding to the separation of redox pairs is found to be insignificant, which is a desirable property for any lithium intercalating electrode to exhibit better electrochemical properties [35]. Further, the electrochemical cycling stability of HDT synthesized $LiMn_2O_4$ cathode upon extended cycling is better understood from the closely overlapping CV peaks (Fig. 7) of the same during the first and after the 20th cycle.

F. Charge-Discharge Behavior

Fig. 8 shows the charge/discharge behavior of the $LiMn_2O_4$ cathode at C/20 rate. The initial discharge capacity of $Li|electrolyte|LiMn_2O_4$ cell is around 118 $mAhg^{-1}$, which is found to decline to 104 $mAhg^{-1}$ after 50 cycles, with a capacity loss of 11.83%. Herein, an initial capacity loss of 9.0% is observed up to 10 cycles and a reduced capacity loss of about 2.8% is observed from 11–50 cycles. Such a decreasing discharge behavior during first few cycles and the progressively stabilized capacity behavior of $LiMn_2O_4$ cathode are already reported [36], [37]. It is well known that the decreasing discharge capacity values of $LiMn_2O_4$ cathode upon cycling may be corroborated to the dissolution of Mn^{3+} into the electrolyte and also to the Jahn-Teller effect associated with the Mn^{3+} ions in the lattice [38], [39].

However, the magnitude of specific capacity exhibited by HDT synthesized $LiMn_2O_4$ cathode (118 mAh g^{-1}) is found to be better than the microemulsion [37] synthesized (100 mAh g^{-1}) and solid-state [38] synthesized (90–100 mAh g^{-1}) $LiMn_2O_4$ and is in closer agreement with the commercial sample [40] reported by Park *et al.* (115 mAh g^{-1}) and the ceramic process synthesized $LiMn_2O_4$ cathode [41] (115 mAh g^{-1}). Hence, the dependence of discharge capacity values on the method of preparation of $LiMn_2O_4$ compound, as reported by Sinha *et al* [37], is understood from the present study also. In addition, a progressively increasing coulombic efficiency behavior of $LiMn_2O_4$ cathode [37], [39] is observed (Fig. 8), which may be correlated to the advantages of HDT synthesis method in producing nanocrystalline $LiMn_2O_4$ particles that reduces the capacity fade upon cycling via improved and facile lithium diffusion kinetics.

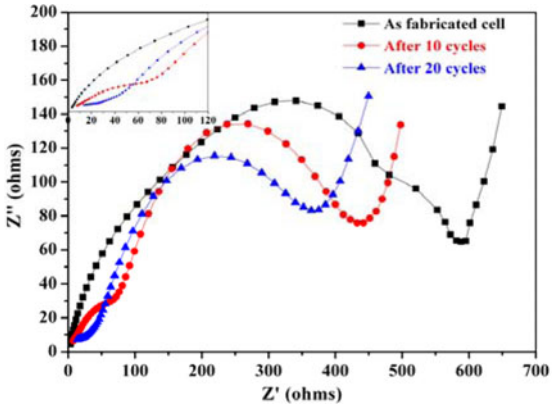

Fig. 9. Nyquist plot of $LiMn_2O_4$ recorded after different cycles.

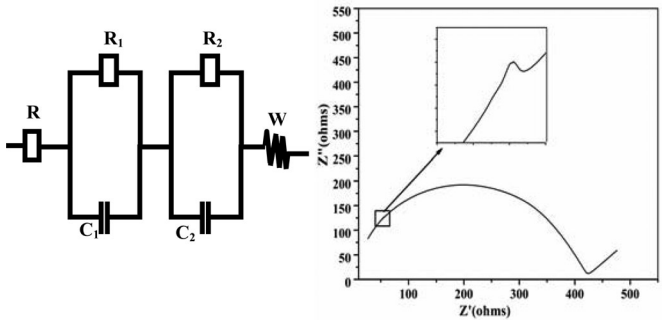

Fig. 10. (a) Proposed equivalent circuit model and (b) simulated impedance spectra of $LiMn_2O_4$ cathode.

G. Impedance Measurements

Nyquist plots of the spinel $LiMn_2O_4$ cathode after different cycles are shown in Fig. 9. Each Nyquist plot is composed of deformed semicircle region in high and medium frequencies and a Warburg region followed by a steep sloping line at the lowest frequencies [42]. The first semicircle (at high-frequency region) is ascribed to lithium-ion diffusion through the surface layer, the second semicircle (at medium-to-low frequency region) is assigned to charge-transfer reaction, and the slope at the low-frequency region is attributed to the solid state diffusion of lithium ion in the active material [43].

It is evident from Fig. 9 that the width of the first semicircle decreases and the width of the second semicircle increases with the increasing number of cycles. The reduced width of the first semicircle is attributed to the advantageous effect of nanocrystalline nature of $LiMn_2O_4$ cathode and the same is an indication of significantly reduced resistance of lithium diffusion that occurs through the surface layer. The increasing charge-transfer resistance of $LiMn_2O_4$ cathode upon cycling (enlarged second semicircle) attributes to the unavoidable fade in capacity observed with the currently synthesized $LiMn_2O_4$ cathode. However, the total internal resistance of the cell decreases with the increasing number of cycles, which is in accordance with the reduced capacity fade behavior of nanocrystalline $LiMn_2O_4$ cathode upon cycling.

In order to simulate the lithium intercalation behavior of $LiMn_2O_4$ cathode, a possible equivalent circuit model is proposed and the same is depicted in Fig. 10(a). Fig 10(b) corresponds to the simulated impedance spectra and evidences the fact that the simulated intercalation behavior is in good agreement with the experimentally observed one.

The impedance spectrum in Fig. 10(b) consists of two semicircles corresponding to the two pairs of parallel resistances and capacitances [44]. R is the ohmic electrolyte resistance, R_1 is the resistance for Li^+ ion migration through the surface layer, C_1 corresponds to interfacial capacitance corresponding to R_1, R_2, and C_2, respectively, denote the double-layer capacitance and charge transfer resistance, and W is an infinite length Warburg impedance that reflects the solid-state diffusion of Li^+ ion [45]. It is observed that the proposed equivalent circuit fits with the experimentally observed impedance spectral behavior satisfactorily.

IV. Conclusion

Phase pure and nanocrystalline $LiMn_2O_4$ rods possessing a diameter of 50 nm have been prepared at a temperature as low as 140 °C by adopting H_2O_2-assisted one-pot hydrothermal synthesis, with an excess concentration of Li:Mn precursor ratio (2:1). An in-house made hydrothermal reaction vessel has been exploited in the study, wherein an optimized total volume of 80% of precursor solution containing H_2O_2 is found to be effective in maintaining the internal pressure required to form the product at such a lower temperature of 140 °C. The mixed valent oxidation state of Mn is confirmed from XPS study and the SAED pattern evidences the growth of nanorods along (111) crystallographic direction. The observed capacity of 118 mAh g^{-1} with an acceptable capacity fade noticed upon extended cycling is substantiated from the closely overlapping CV peaks and the decreasing total internal resistance value of Li|electrolyte|$LiMn_2O_4$ cell with the increasing number of cycles. A self-explanatory equivalent circuit model is also proposed for the observed impedance behavior of $LiMn_2O_4$ cathode. The possibility of exploiting hydrothermal method to synthesize nanocrystalline $LiMn_2O_4$ and the effect of nanocrystalline $LiMn_2O_4$ cathode in reducing the diffusion path length and to exhibit desirable lithium intercalation behavior are understood from the study.

References

[1] M. M. Thackeray, Y. Shao-Horn, A. J. Kahaian, K. D. Kepler, E. Skinner, J. T. Vaughey, and S. A. Hackney, "Structural fatigue in spinel electrodes in high-voltage (4 V) $Li/Li_xMn_2O_4$ cells," *Electrochem. Solid-State Lett.*, vol. 1, pp. 7–9, 1998.

[2] J. C. Hunter, "Preparation of a new crystal form of manganese dioxide: λ-MnO_2," *J. Solid State Chem.*, vol. 39, pp. 142–147, 1981.

[3] S. J. Wen, T. J. Richardson, L. Ma, K. A. Striebel, P. N. Ross, and E. J. Cairns, "FTIR spectroscopy of metal oxide insertion electrodes: Capacity fading in secondary $Li/LiMn_2O_4$ cells," *J. Electrochem. Soc.*, vol. 143, no. 5, pp. L136–L138, 1996.

[4] D. Guyomard and J. M. Tarascon, "The carbon/$Li_{1+x}Mn_2O_4$ system," *Solid State Ionics*, vol. 69, pp. 222–237, 1994.

[5] J. M. Tarascon, W. R. McKinnon, F. Coowar, T. N. Bowmer, G. Amatucci, and D. Guyomard, "Synthesis condition and oxygen stoichiometry effects on Li insertion into the spinel $LiMn_2O_4$," *J. Electrochem. Soc.*, vol. 141, pp. 1421–1431, 1994.

[6] Y. Xia, Y. Zhou, and M. Yoshio, "Capacity fading on cycling of 4 V $Li/LiMn_2O_4$ cells," *J. Electrochem. Soc.*, vol. 144, pp. 2593–2600, 1997.

[7] J. H. Lee, J. K. Hong, D. H. Jang, Y. K. Sun, and S. M. Oh, "Degradation mechanisms in doped spinels of $LiM_{0.05}Mn_{1.95}O_4$ (M = Li, B, Al, Co, and Ni) for Li secondary batteries," *J. Power Sources*, vol. 89, p. 7, 2001.

[8] H. W. Ha, N. J. Yun, and K. Kim, "Improvement of electrochemical stability of $LiMn_2O_4$ by CeO_2 coating for lithium-ion batteries," *Electrochim. Acta*, vol. 52, pp. 3236–3241, 2007.

[9] G. L. Che, B. Lakshmi, E. R. Fisher, and C. R. Martin, "Carbon nanotubule membranes for electrochemical energy storage and production," *Nature*, vol. 393, pp. 346–349, 1998.

[10] Y. K. Sun, "Synthesis and electrochemical studies of spinel $Li_{1.03}Mn_2O_4$ cathode materials prepared by a sol-gel method for lithium secondary batteries," *Solid State Ionics*, vol. 100, pp. 115–125, 1997.

[11] P. Kalyani, N. Kalaiselvi, and N. Muniyandi, "A new solution combustion route to synthesize $LiCoO_2$ and $LiMn_2O_4$," *J. Power Sources*, vol. 111, pp. 232–238, 2002.

[12] W. Liu, G. C. Farrignton, and F. Chaput, "Synthesis and electrochemical studies of spinel phase $LiMn_2O_4$ cathode materials prepared by the pechini process," *J. Electrochem. Soc*., vol. 143, pp. 879–884, 1996.

[13] T. H. Wang, W. S. Um, and H. S. Lee, "Powder synthesis and electrochemical properties of $LiMn_2O_4$ prepared by an emulsion-drying method," *J. Power Source*, vol. 74, pp. 169–174, 1998.

[14] Y. C. Zhang, H. Wang, H. Y. Xu, B. Wang, H. Yan, A. Ahniyaz, and M. Yoshimura, "Low-temperature hydrothermal synthesis of spinel-type lithium manganese oxide nanocrystallites," *Solid State Ionics*, vol. 158, pp. 113–117, 2003.

[15] S. H. Kang and J. B. Goodenough, "$LiMn_2O_4$ spinel cathode material showing no capacity fading in the 3 V range," *J. Electrochem. Soc*., vol. 147, pp. 3621–3627, 2000.

[16] M. Nishizawa, K. Mukai, S. Kuwabata, C. R. Martin, and H. Yamada, "Template synthesis of polypyrrole-coated spinel LiMn2O4 nanotubules and their properties as cathode active materials for lithium batteries," *J. Electrochem. Soc*., vol. 144, pp. 1923–1927, 1997.

[17] N. Li, C. J. Patrissi, G. L. Che, and C. R. Martin, "Rate capabilities of nanostructured $LiMn_2O_4$ electrodes in aqueous electrolyte," *J. Electrochem. Soc*., vol. 146, no. 6, pp. 2044–2049, 2000.

[18] L. Zhang, J. C. Yu, A. W. Xu, Q. Li, K. W. Kwong, and L. A. Wu, "Self-seeded, surfactant-directed hydrothermal growth of single crystalline lithium manganese oxide nanobelts from the commercial bulky particles," *Chem. Comm*., pp. 2910–2911, 2003.

[19] H. Liu and L. Tan, "A novel method for preparing lithium manganese oxide nanorods from nanorod precursor," *J. Nanopart. Res*., vol. 12, pp. 301–305, 2010.

[20] Z. Liu, W. L. Wang, X. Liu, M. Wu, D. Li, and Z. Zeng, "Hydrothermal synthesis of nanostructured spinel lithium manganese oxide," *J. Solid State Chem*., vol. 177, pp. 1585–1591, 2004.

[21] Gangulibabu, D. Bhuvaneswari, N. Kalaiselvi, N. Jayaprakash, and P. Periasamy, "CAM sol–gel synthesized $LiMPO_4$ (M = Co, Ni) cathodes for rechargeable lithium batteries," *J. Sol-Gel Sci. Technol*., vol. 49, pp. 137–144, 2009.

[22] G. Panasyuk, I. Voroshilov, G. Boudova, L. Azarova, V. Privalov, V. Minin, A. Skundin, L. Kanevsky, T. Kulova, M. Danchevskaya, and Y. Ivaki, "Synthesis of lithium-manganese oxide spinel in hydrothermal conditions," *High Pressure Res*., vol. 20, pp. 39–43, 2001.

[23] A. Vadivel Murugan, B. Kale, B. Lalita, B. Kunde, Aarti, and V. Kulkarni, "Comparison of different soft chemical routes synthesis of nanocrystalline $LiMn_2O_4$ and their influence on its physicochemical properties," *J. Solid State Electrochem*., vol. 10, pp. 104–109, 2006.

[24] H. M. Wu, J. P. Tu, Y. F. Yuan, Y. Li, W. K. Zhang, and H. Huang, "Electrochemical performance of nanosized $LiMn_2O_4$ for lithium-ion batteries," *Physica B*, vol. 369, pp. 221–226, 2005.

[25] G. T. Chandrappa, N. Steunou, S. Cassaignon, C. Bauvais, and J. Livage, "Hydrothermal synthesis of vanadium oxide nanotubes from V_2O_5 gels," *Catalysis Today*, vol. 78, pp. 85–89, 2003.

[26] D. K. Kim, P. Muralidharan, H. W. Lee, R. Ruffo, Y. Yang, C. K. Chan, H. Peng, R. A. Huggins, and Y. Cui, "Spinel $LiMn_2O_4$ nanorods as lithium ion battery cathodes," *Nano Lett*., vol. 8, no. 11, pp. 3948–3952, 2008.

[27] C. M. Julien and M. Massot, "Local structure of manganese oxides and lithium intercalates," *Ionics*, vol. 11, pp. 226–235, 2005.

[28] C. M. Julien and M. Massot, "Spectroscopic studies of the local structure in positive electrodes for lithium batteries," *Phys. Chem. Chem. Phys*., vol. 4, pp. 4226–4235, 2002.

[29] X. Liu, J. Wang, J. Zhang, and S. Yang, "Fabrication and characterization of Zr and Co co-doped $LiMn_2O_4$ nanowires using sol-gel AAO template process," *J. Mater. Sci.: Mater Electron*., vol. 17, no. 11, 461, pp. 865–870, 2006.

[30] C. V. Ramana, M. Massot, and C. M. Julien, "XPS and Raman spectroscopic characterization of $LiMn_2O_4$ spinels," *Surf. Interface Anal*, vol. 37, pp. 412–416, 2005.

[31] D. W. Shin, J. W. Choi, W. K. Choi, Y. S. Cho, and S. J. Yoon, "XPS/EXAFS study of cycleability improved $LiMn_2O_4$ thin film cathodes prepared by solution deposition," *Electrochem. Commun*., vol. 11, pp. 695–698, 2009.

[32] X. Li and Y. Xu, "Novel method to enhance the cycling performance of spinel $LiMn_2O_4$," *Electrochem. Commun*., vol. 9, pp. 2023–2026, 2007.

[33] L. Hernán, J. Morales, L. Sánchez, and J. Santos, "Electrochemical properties of defective $Li_{1-x}Mn_{2-\delta}O_4$ spinels prepared by a solgel method used as cathodes in lithium cells," *Solid State Ionics*, vol. 1043, no. 4, pp. 205–213, 1997.

[34] S. B. Tang, H. Xia, M. O. Lai, and L. Lu, "Characterization of $LiMn_2O_4$ thin films grown on Si substrates by pulsed laser deposition," *J. Alloys and Compounds*, vol. 449, pp. 322–325, 2008.

[35] V. G. Kumar, J. S. Gnanaraj, S. Ben-David, M. D. Pickup, R. H. Ernst van-Eck, A. Gedanken, and D. Aurbach, "An aqueous reduction method to synthesize spinel-$LiMn_2O_4$ nanoparticles as a cathode material for rechargeable lithium-ion batteries," *Chem. Mater*., vol. 15, pp. 4211–4216, 2003.

[36] D. Liu, Z. He, and X. Liu, "Increased cycling stability of $AlPO_4$-coated $LiMn_2O_4$ for lithium ion batteries," *Mater. Lett*., vol. 61, pp. 4703–4706, 2007.

[37] N. N. Sinha and N. Munichandraiah, "Synthesis and characterization of submicron size particles of $LiMn_2O_4$ by microemulsion route," *J. Solid State Electrochem*., vol. 12, pp. 1619–1627, 2008.

[38] D. S. Ahn and M. Y. Song, "Variations of the electrochemical properties of $LiMn_2O_4$ with synthesis conditions," *J. Electrochem. Soc*., vol. 147, pp. 874–879, 2000.

[39] Z. Liu, A. Yu, and J. Y. Lee, "Cycle life improvement of $LiMn_2O_4$ cathode in rechargeable lithium batteries," *J. Power Sources*, vol. 74, pp. 228–233, 1998.

[40] S. C. Park, Y. M. Kim, Y. M. Kang, K. T. Kim, P. S. Lee, and J. Y. Lee, "Improvement of the rate capability of $LiMn_2O_4$ by surface coating with $LiCoO_2$," *J. Power Sources*, vol. 103, pp. 86–92, 2001.

[41] M. Lanz, C. Kormann, H. Steninger, G. Heil, O. Hass, and P. Noavak, "Large-agglomerate-size lithium manganese oxide spinel with high rate capability for lithium-ion batteries," *J. Electrochem. Soc*., vol. 147, pp. 3997–4000, 2000.

[42] S. B. Tang, M. O. Lai, and L. Lu, "Properties of nano-crystalline $LiMn_2O_4$ thin films deposited by pulsed laser deposition," *Electrochim. Acta*, vol. 52, pp. 1161–1168, 2006.

[43] J. Liu and A. Manthiram, "Understanding the improvement in the electrochemical properties of surface modified 5 V $LiMn_{1.42}Ni_{0.42}Co_{0.16}O_4$ spinel cathodes in lithium-ion cells," *Chem. Mater*., vol. 21, pp. 1695–1707, 2009.

[44] P. Suresh, A. K. Shukla, and N. Munichandraiah, "Temperature dependence of ac impedance in lithium-ion cells," *J. Appl. Electrochem*., vol. 32, pp. 267–273, 2002.

[45] L. Xifei and X. Youlong, "Novel method to enhance the cycling performance of spinel $LiMn_2O_4$," *J. Electrochem. Commun*., vol. 9, pp. 2023–2026, 2007.

Authors' photographs and biographies not available at the time of publication.